Ni/Si(111) system: Formation and evolution of two- and three-dimensional phases studied by spectromicroscopy

L. Gregoratti and S. Günther
Sincrotrone Trieste, Area Science Park, 34012 Basovizza, Trieste, Italy

J. Kovaĉ
Institute of Surface Engineering and Optoelectronics, Teslova 30, 3000 Ljubljana, Slovenia

M. Marsi
Sincrotrone Trieste, Area Science Park, 34012 Basovizza, Trieste, Italy

R. J. Phaneuf
Department of Physics, University of Maryland, College Park, Maryland 20742-4111

M. Kiskinova
Sincrotrone Trieste, Area Science Park, 34012 Basovizza, Trieste, Italy
(Received 27 July 1998)

The spatial variations in the composition and electronic structure of Ni/Si interfaces formed via reactive epitaxy at 830 K and successively annealed to 950 K have been studied by synchrotron-radiation scanning photoelectron microscopy, a method that combines chemical mapping with photoelectron spectroscopy from selected spots of the surface. The combination of submicron spatial resolution ($\leqslant 0.15\ \mu$m) with high energy resolution allowed us to characterize the coexisting phases including micron-sized silicide islands and two-dimensional structures. Deposition of 0.7 ML Ni at 830 K produced domains of the $\sqrt{19}$ phase with different Ni concentration, coexisting with NiSi and $NiSi_2$ islands. Annealing this interface to 950 K led to conversion of the $\sqrt{19}$ to a (1×1)-RC structure (where RC is ring cluster), which appears to be more uniform than the $\sqrt{19}$ surface. From the chemical maps and the Si *2p*, Ni *3p*, and valence-band spectra corresponding to the coexisting phases the nature of the phases was determined and the mechanism of the Ni mass transport on the $\sqrt{19}$ and (1×1)-RC surfaces was examined. [S0163-1829(99)08903-1]

I. INTRODUCTION

The Ni/Si interface is a typical example of a system in which there occur a number of surface phases and bulk equilibrium Ni_xSi_y compounds ($x=1,2,3,5$; $y=1,2$), growing nearly epitaxially on the Si substrate.[1] The nucleation and growth of the two- (2D) and three- (3D) dimensional phases in the initial stages of formation of Ni/Si interfaces, prepared by reactive epitaxy (RE) or solid phase epitaxy (SPE), have been extensively studied by means of structural or microscopy techniques, such as low-energy electron diffraction (LEED), low-energy electron microscopy (LEEM), transmission or secondary electron microscopy (TEM or SEM), reflection high energy electron diffraction (RHEED), scanning tunnelling microscopy (STM).[1–4] Among the several 2D phases reported in the literature [$(\sqrt{3}\times\sqrt{3})R30°$, $(\sqrt{19}\times\sqrt{19})R23.4°$, and (1×1)-RC], which involve different reconstructions of the Si(111) surface, the $\sqrt{19}$ and the (1×1)-RC phases were suggested as the most likely intermediate steps to epitaxial growth of 3D $NiSi_2$.[2,3] It is known from previous studies that a rather complex surface morphology with 3D islands coexisting with 2D structures occurs at elevated temperatures, when the Ni coverage exceeds a few tenths of monolayer.[1–4] However, the above-mentioned techniques cannot provide the necessary quantitative information to identify unambiguously the composition of the phases, because of their limited spectroscopic capabilities.

We used synchrotron radiation scanning photoemission microscopy (SR-SPEM) to identify the composition and electronic structure of the coexisting 2D and 3D phases formed during the initial stages of the RE nickel silicide growth. The present paper is on the composition of an interface formed by RE deposition of 0.7 ML Ni and its evolution after annealing ~950 K. This temperature is lower than the temperature (>1000 K) at which the silicide islands and Ni dissolve into the bulk.[3] The present study follows our earlier SR-SPEM characterization of a similar Ni/Si interface but formed by SPE at temperatures of 1150 K, above the Ni solvus line.[5] In this case the dissolved Ni driven to the surface upon cooling formed (1×1)-RC and silicide islands. Comparison of the interfaces formed under different formation conditions has allowed us to correlate the growth of the silicide islands with the spatial evolution of the 2D $\sqrt{19}$ and (1×1)-RC phases developed outside the islands. This study also appears to be the first photoemission spectroscopy characterization of the $\sqrt{19}$ and (1×1)-RC surfaces.

II. EXPERIMENT

The experiments were performed at the ESCA microscopy beamline on the ELETTRA synchrotron light source, which hosts the scanning photoemission microscope (SPEM). Basic components of the microscope are the photon

focusing system (a combination of a Fresnel zone plate lens and an order sorting aperture), specimen positioning and scanning systems and hemispherical capacitor electron analyzer of a $\pm 15°$ acceptance angle, at grazing angle with respect to the incident beam and sample normal. The microscope can operate in two modes: imaging and spectroscopy. The variation in the contrast of the images obtained by detecting the photoelectron yield from a selected atomic core level reflects the spatial variation of the elemental concentration or elemental chemical state. The measurement station has a preparation chamber equipped with LEED, cylindrical mirror analyzer and all necessary facilities for sample cleaning, metal deposition, etc. A detailed description of the beamline and measurement station can be found in Ref. 6.

Prior to Ni deposition the Si(111) samples (cut from *n*-doped wafers) were cleaned by flashing to 1500 K followed by slowly raising and lowering the temperature through approximately 1150–1400 K until a sharp (7×7) LEED pattern was observed. Water cooled electron beam evaporators equipped with a flux monitor were used for Ni deposition. The amount of the deposited Ni was controlled by measuring the Si(KLL) and Ni(LMM) Auger and the Ni *3p* and Si *2p* photoelectron (PE) yields. The appearance of sharp $\sqrt{19} \times \sqrt{19}$ reflections in the LEED pattern at coverage of 0.16 ML was used for Ni coverage calibration. The initial interface in the present study was obtained by Ni deposition on a Si(111)-7×7 sample at 830 K. The LEED pattern of this interface showed a sharp multidomain $\sqrt{19}$ pattern. We followed the evolution of the interface after annealing to ~950 K during which the $\sqrt{19}$ converted to a (1×1)-RC structure.

The present SPEM experiments were carried out with photon energy of 500 eV. The lateral resolution in the present measurements was 0.15 μm and the overall energy resolution was 0.34 eV, better than that used in our previous SPE studies.[5] This helped us to improve the fitting procedure and extract more information about the chemical composition of the coexisting phases. The escape depth for the Si *2p* and Ni *3p* photoelectrons was estimated using the universal curve for electron mean free path,[7] ~9 Å at 400–450 eV, and the takeoff angle of the analyzer ~65° with respect to the normal incident beam. This gives an effective escape depth of ~4 Å, i.e., for the present experimental setup the probe depth is less than 20 Å. The correction of the chemical maps for possible topographical artifacts was made using the procedures described in Refs. 6 and 8.

III. RESULTS

Figures 1(a) and 1(b) show a typical Ni *3p* chemical map of the initial Ni/Si surface, on which we observed a $\sqrt{19}$ LEED pattern. The contrast levels of the maps reflect the variations in the Ni content at the surface and near-surface region. In particular, the compact bright features of micron dimensions are relatively Ni rich, whereas the remaining dark parts of the image can be associated with lower Ni composition. As will be shown below, the PE spectra identify the bright features in Figs. 1(a) and 1(b) as silicide 3D islands, and the surrounding darker regions as 2D ordered phase with varying Ni content. Clearly two different shapes of islands can be distinguished: ''long'' islands, elongated along the ⟨110⟩ directions, and ''quasi-isotropic'' islands,

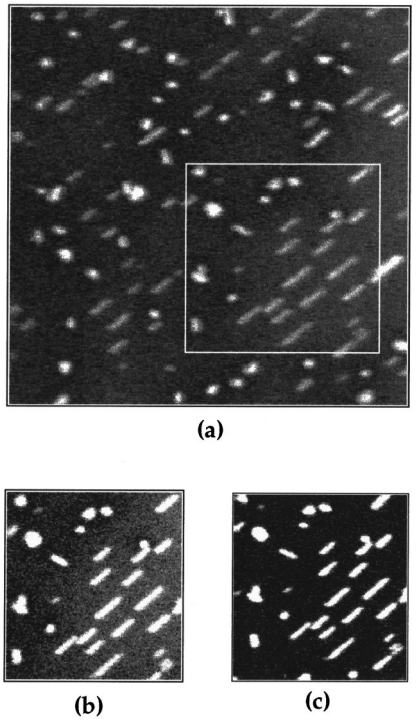

FIG. 1. (a) 59×59 μm^2 Ni *3p* map from the Ni/Si interface formed at 830 K; (b) and (c) 26×26 μm^2 fraction of the Ni *3p* map in (a) illustrating the change of the gray level of the 2D phase after annealing the 830 K Ni/Si interface (b) to 950 K (c).

among them triangular or hexagonal-shaped ones. The islands cover ~6% of the surface and contain at least 0.54 ML of Ni, assuming for the $\sqrt{19}$ phase, covering the rest of the surface, the maximum Ni coverage of 0.16 ML.[2] This means that on average each island contains ~9 ML of Ni, which means an average thickness of the $NiSi_2$ islands ~30 Å, considering the cubic $NiSi_2$ structure.[1]

Figure 1(c) shows the same region as Fig. 1(b) after annealing at 950 K. The visible difference is that the dark regions, now converted into a (1×1)-RC phase according to the LEED pattern, are with a reduced and almost uniform gray level.

The varying intensity level of the dominating dark regions in Figs. 1(a) and 1(b) indicates a laterally varying Ni density. Assuming that the highest intensity corresponds to the perfect $\sqrt{19}$ phase containing ~0.16 ML of Ni we used this value for normalization of the Ni coverage. The obtained values of the gray levels for the Ni *3p* maps range from 0.5 to 1.0. Close examination shows that the darkest areas contain a higher density of quasi-isotropic islands. The (1×1)-RC phase in Fig. 1(c) appears to be more uniform within our lateral resolution: the gray value of 0.5 ± 0.05 was measured. Note that the (1×1)-RC phase also can be of a variable Ni density but this inhomogeneity is at a smaller spatial scale.[2,3] The gray scale values are consistent with the model, proposed in Ref. 2, where Ni concentration in the (1×1)-RC phase is indeed smaller than in the $\sqrt{19}$ phase. Since the $\sqrt{19}$ and (1×1)-RC phases can be observed in a rather wide Ni coverage range [0.08–0.16 ML for $\sqrt{19}$ and 0.03–0.13 ML for (1×1)[3]] we cannot determine unambiguously from the maps whether the variations in the Ni con-

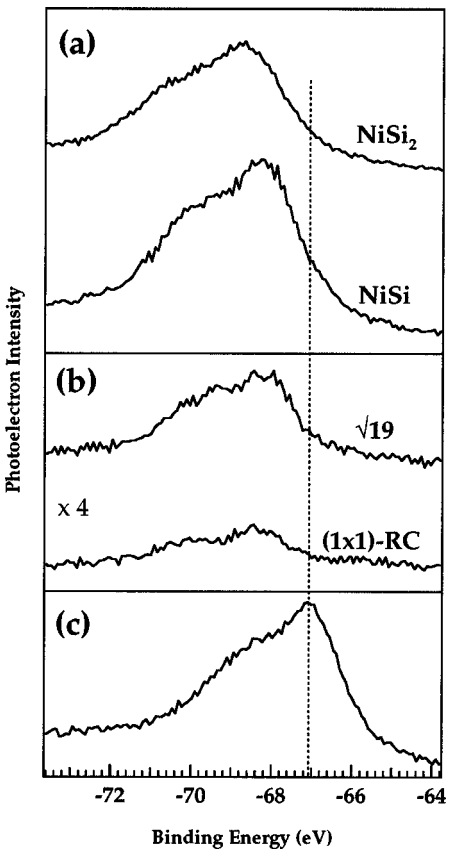

FIG. 2. Ni *3p* spectra taken from the islands (a), the $\sqrt{19}$ and (1×1)-RC areas away of the islands (b), and metallic nickel (c). The dashed line indicates the position of Ni $3p_{3/2}$ metallic line.

centration in Fig. 1(a) are due to (i) large domains of $\sqrt{19}$ reconstructions with different ''light wall''-type defects or (ii) coexistence of $\sqrt{19}$ and (1×1)-RC areas. As will be shown below the PE spectra taken from the different gray regions in Fig. 1(a) support (i).

The Ni *3p*, Si *2p*, and valence-band (VB) PE spectra taken from the silicide islands and 2D structures were excellent fingerprints for the composition and electronic structure of the coexisting phases.

Figure 2 shows selected Ni *3p* PE spectra taken from different spots of the images in Figs. 1(b) and 1(c). The energy positions of the Ni *3p* levels are shifted with respect to the metallic Ni position (bottom spectrum) by different amounts, reported in Table I. The Ni *3p* chemical shift is the same (within accuracy ±0.05 eV) for both 2D structures. The intensity of the Ni *3p* spectra varied in correspondence with the gray scale of the Ni *3p* maps. In order to reduce the influence of the photon flux and photoelectron angular distribution on the determination of the relative Ni content in the phases we used the Ni *3p*/Si *2p* area ratio, $I_{\mathrm{Ni}}/I_{\mathrm{Si}}$. The evaluated $I_{\mathrm{Ni}}/I_{\mathrm{Si}}$ values are reported in Table I. The values and the variations of $I_{\mathrm{Ni}}/I_{\mathrm{Si}}$ ratios are consistent with the gray scales in Fig. 1. As will be shown below the presence of an out-diffused Si layer of varying thickness, which wets the top of the $NiSi_2$ islands, accounts for the differences of the corresponding $I_{\mathrm{Ni}}/I_{\mathrm{Si}}$ values.

Figures 3 and 4 show representative Si *2p* and VB spectra of the $NiSi_2$ and NiSi islands and the 2D phases, from spots selected from the maps shown in Figs. 1(b) and 1(c). The Ni *3d*-derived states dominate the VB spectra of the islands. The peak at ~3.1 eV for the ''long'' islands is a distinctive feature of the VB of the $NiSi_2$ phase, whereas quasi-isotropic islands are characterized by a broader structure resembling a doublet with maxima at ~ -1.8 and -2.7 eV, typical of the NiSi phase.[1] Closer examination of the spectra in Fig. 3 taken from the different $NiSi_2$ islands reveals that the sharpness of the 3.1-eV peak and the relative intensity of the shoulder on the higher binding energy tail due to Si-*3p* contribution, varies in concert with the changes of the Si *2p* line shape. No such differences were observed in the VB and Si *2p* spectra from the NiSi islands. Despite the much lower Ni concentration the Ni *d* states also contribute to the overall intensity at ⩽4 eV in the VB spectra of the 2D phases shown in Fig. 4. The VB of both phases exhibit a very low intensity at the Fermi level and a rigid onset energy shift by ~ -0.2 eV with respect to the valence bands of the 3D phases. As expected, the relative intensity of the Si-derived *3s* (~8 eV) and *3p* (~4 eV) states in the VB spectra from the 2D phases is substantially enhanced. The Si-derived states are more intense in the (1×1)-RC spectra consistent with its microscopic structure containing regions of Ni-free Si domains.[3]

With small exceptions, the Si *2p* and VB spectra of the $NiSi_2$ and NiSi islands, shown in Fig. 3, are similar to the spectra of the silicide islands formed by SPE at 1150 K,[5] but the improved energy resolution in the present measurements has allowed us to perform more precise deconvolution of the spectra. The fitting of the Si *2p* spectra was performed using Doniach-Sunjic functions convoluted with Gaussians, which

TABLE I. Binding energy shifts in eV for the reacted, $\Delta E_b(R)$, and ''surface,'' $\Delta E_b(S1)$ and $\Delta E_b(S2)$ components of the Si *2p* spectra (columns 1–3) and ΔE_b(Ni) of the Ni *3p* levels (column 4). Columns 5–8 show the $I_{\mathrm{Ni}}/I_{\mathrm{Si}}$ ratio and the relative weight of the Si *2p* fitting components. I_{Si} is for the total Si *2p* intensity. In brackets the calculated values of the relative yield of the differently coordinated Si atoms assuming ''close-packed'' $\sqrt{19}$ and (1×1)-RC structures are quoted.

Phase	$\Delta E_b(R)$	$\Delta E_b(S1)$	$\Delta E_b(S2)$	ΔE_b(Ni)	$I_{\mathrm{Ni}}/I_{\mathrm{Si}}$	I_{S1}/I_{Si}	I_{S2}/I_{Si}	I_R/I_{Si}
$NiSi_2$	-0.55 ± 0.05	+0.55		-1.0 ± 0.1	0.6–1.4	0–0.03		0.40–0.60
NiSi	−0.10	+0.25	+0.38	-0.7 ± 0.1	1.0–1.2	0.20	0.10	0.70
$\sqrt{19}$	−0.44	+0.46		-0.6 ± 0.1	⇐0.03	0.21		0.14
(calc.)						(0.08)		(0.11)
(1×1)	−0.45	+0.3	+0.73	-0.6 ± 0.1	⇐0.01	0.20	0.06	0.11
(calc.)						(0.12)	(0.03)	(0.12)

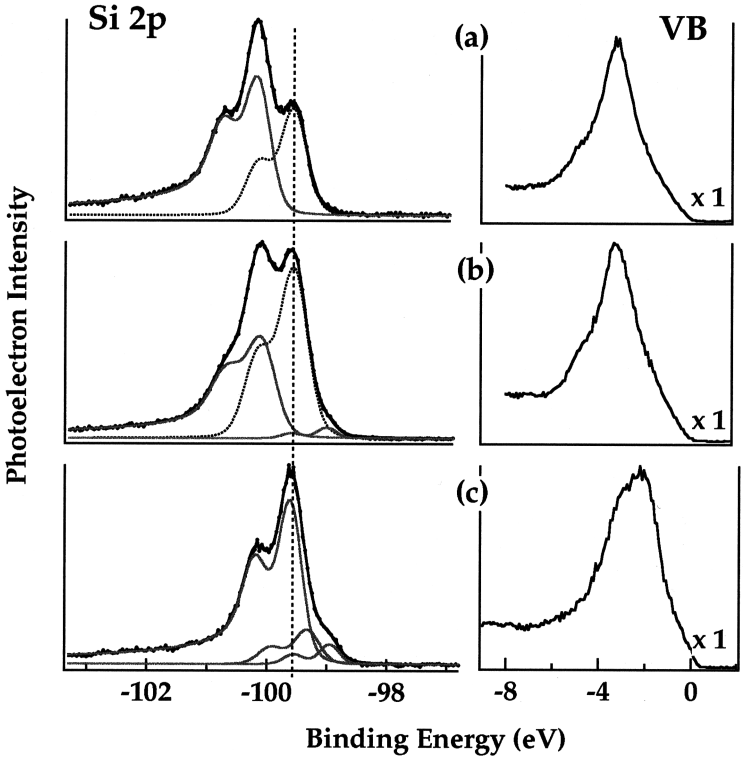

FIG. 3. Si *2p* and VB spectra taken from: (a) and (b) long $NiSi_2$ islands with different thickness of the Si unreacted layer; (c) quasi-isotropic NiSi-like island. The fitting components are plotted as well. The dashed line indicates the position of bulk Si $2p_{3/2}$ component (plotted by dotted lines) of the $NiSi_2$ islands.

simulate the overall energy spread. The optimized fitting parameters are reported in Table II. The shake-up events occurring following excitations of metalliclike phases[9] account for the asymmetry of the reacted Si component, attributed to Si atoms coordinated with Ni. The positions and the relative weight of the different components derived from the Si *2p* line shape analyses are reported in Table I. Most of the Si *2p* spectra from the $NiSi_2$ islands require three components: one coincident with the bulk Si position, one reacted component *R* and a third weak component *S1* fitting the low binding energy shoulder, which can be clearly distinguished in the spectrum of Fig. 3(b). Since the thickness of the $NiSi_2$ islands exceeds the probed depth, the ''bulk'' component is identified as unreacted epitaxial Si layer on top of the is-

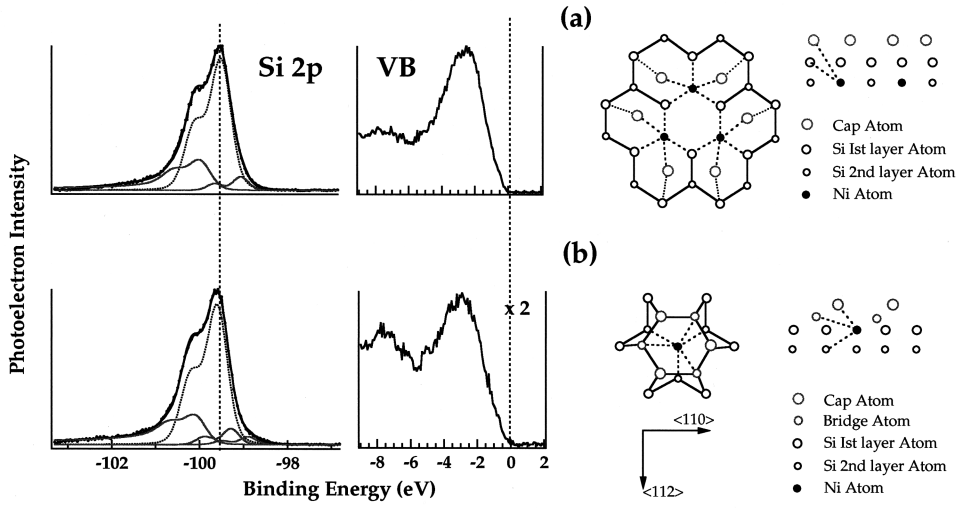

FIG. 4. Si *2p* and VB spectra taken from out-of-island $\sqrt{19}$ (a) and (1×1)-RC (b) structures. The fitting components are plotted as well. The dashed line indicates the position of the bulk Si $2p_{3/2}$ component (plotted by dotted lines), of the $\sqrt{19}$ phase. The suggested structural models of the $\sqrt{19}$ and (1×1)-RC phases are shown on the right side (Ref. 2).

TABLE II. Parameters used for fitting of the Si *2p* spectra shown in Fig. 3.

Phase	Si_{bulk}	*R*	*S1*	*S2*
		$NiSi_2$		
Gaussian	0.49	0.46	0.33	
Asymmetry	0	0.2	0	
		NiSi		
Gaussian		0.35	0.35	0.34
Asymmetry		0.25	0	0
		$\sqrt{19}$		
Gaussian	0.5	0.5	0.36	
Asymmetry	0	0.18	0	
		(1×1)		
Gaussian	0.5	0.5	0.38	0.38
Asymmetry	0	0.26	0	0

lands, the formation of which is favored by the lower surface energy of Si than that of $NiSi_2$.[10,11] The relative weight of this bulk component varies substantially with the different $NiSi_2$ islands (corresponding to a coverage up to 2 ML) and accounts for the different Si *2p* line shapes in Figs. 3(a) and 3(b). In accordance with the previous studies it is natural to assign the *S1* component to the Si adatoms of the (2×2) surface structure, observed by RHEED and STM,[2–5] which is formed on top of the epitaxial Si layer covering the $NiSi_2$ islands. The weight of *S1* varies in concert with the bulk component: it is practically absent in the spectra with the thinnest Si layer [see spectrum (a) in Fig. 3]. This result means that the formation of the adatom structure requires more than one epitaxial Si layer on top of the islands. A very similar shoulder was observed in the spectra of the Si(111)-2×1 surface, which was attributed to emission from the surface Si adatoms.[12]

Fitting the Si *2p* spectra of the NiSi islands always requires three components, a dominant *R* component and two weaker *S1* and *S2* components. In contrast to the case of the $NiSi_2$ islands all NiSi islands show the same Si *2p* lineshape indicating the same composition of the top layers. The origin of the *S1* and *S2* components is not clear: they carry ~0.3 of the total peak intensity, which corresponds to ~1 ML. We note that the Si *2p* spectra of the NiSi islands formed by RE at 830 K contain a more pronounced lower BE shoulder than those produced by SPE at 1150 K, which translates into an increased contribution of the *S2* component at the expense of the *S1* one. Comparison of the present results with the previous SPE results indicates that the relative ratio between *S1* and *S2* changes with formation conditions, whereas their total intensity always corresponds to ~1 ML. This prompts us to suggest that *S1* and *S2* components are induced by segregated Si surface atoms with two different environments that might be an intermediate step in the conversion to the Si rich $NiSi_2$ phase.

A distinctive feature of the Si *2p* spectra from the 2D phases in Fig. 4, where the dominant component is unreacted Si, is that compared to Si(111)-7×7 and $NiSi_2$ the Si *2p* bulk position is shifted to higher binding energy, by −0.11 eV for the $\sqrt{19}$ and −0.23 eV for the (1×1)-RC structure. These shifts we attribute to Schottky-barrier-height variations related to variations of the surface composition and structure. The important result is that the energy position of the Si *2p* spectra from the out-of-island areas of the initial interface does not change with the variations of the local Ni concentration. The parameters of the other fitting components due to emission from Si in an environment different from bulk Si are reported in Table I. Excepting the leading bulk Si component, the decomposition of the Si *2p* spectra of both 2D phases results in a higher BE component *R* attributed to Si bonded to Ni, and two lower binding energy components *S1* and *S2*.

IV. DISCUSSION

A. PE from the 2D phases

To our knowledge photoemission spectra for the $\sqrt{19}$ and (1×1)-RC Ni reconstructions on Si(111) have not been reported yet. Here we make the first attempt to examine the features in the decomposed Si *2p* spectra and assign them to the different chemical environments of the Si atoms in the phases. For both phases the leading peak corresponds to unreacted Si, the energy position of which is shifted slightly by different amount to higher binding energies. The direction of the shift is consistent with the slight shifts in the corresponding VB spectra. The different amount of the shift for the $\sqrt{19}$ and (1×1)-RC phases reflects the effect of the interface atomic structure on the Fermi-level pinning. The 2D phases under investigation have atomic arrangement with sixfold coordinated Ni in a substitutional place in the bottom ($\sqrt{19}$) or top ((1×1)-RC) of the substrate bilayer (see the models drawn in Fig. 4). The shift of the unreacted Si *2p* peak is smaller than the measured −0.6 eV for the Ni *3p* levels. This means that the Ni *3p* shift involves a pure chemical shift as well, which is larger for the $\sqrt{19}$ phase. The shortest Ni-Ni distance is ~3.7 Å (two first neighbors) for the $\sqrt{19}$ and ~10.2 Å (six first neighbors) for the (1×1)-RC phase. This clearly shows that there is no correlation between the Ni *3p* chemical shift and the Ni-Ni distances contrary to the reports for the different 3D silicide phases,[13] where the amount of the shift increases with the increase of the Ni-Ni separation. Excepting the emission from the unreacted Si, which gives ~2/3*ds* of the PE intensity, the unit cells of the $\sqrt{19}$ and (1×1)-RC phases have the following chemical environments for the remaining Si atoms. For the $\sqrt{19}$ structure four Si atoms from the bilayer are bonded to each Ni (48 atoms for each unit cell) and six Si adatoms are bridge-bonded between Ni and Si from the top layer, forming a ring consisting of three dimers (24 atoms for a unit cell). For the (1×1)-RC phases there are two kinds of Si atoms bonded to Ni: three Si atoms from the bottom of the bilayer and three out of the six adatoms, which formed a buckled hexagonal ring. The remaining three Si adatoms, called ''cap'' atoms are not bonded to Ni.

The best fit to the relative intensities of the shifted components of the Si *2p* spectra are in fair agreement with those expected from the model structures of the phases, although there are deviations from the yields, calculated assuming

saturation coverage for the $\sqrt{19}$ and (1×1) structures and reported in brackets in Table I. For the $\sqrt{19}$ phase in addition to the bulk component there are two more components: the *R* component we assign to the four Si atoms from the bilayer bonded to Ni whereas the *S1* component to emission from the six Si adatoms. For the (1×1)-RC the components are three: one *R* and two higher binding energy components tentatively identified with the different environment of the Si adatoms in the ring. From the above models, proposed by Bennett and co-workers,[2–4] the atomic arrangement of the (1×1)-RC resembles more the $NiSi_2$ environment. However, for both phases the amount of the *R* shift is comparable with those of the $NiSi_2$ phase. The difference in the energy positions and line shapes of the Si *2p* spectra corresponding to the (1×1)-RC and $\sqrt{19}$ phases rules out the coexistence of $\sqrt{19}$ structure of the initial interface with large (1×1)-RC domains. As noted above the energy position of the Si *2p* spectra from the out-of-island areas of the initial interface does not change with the variations of the local Ni concentration, which is consistent with formation of $\sqrt{19}$ domains with different compression.

B. Composition of the silicide islands and Ni mass transport to the islands from the 2D phases

The present spectromicroscopy study of the Ni/Si interface formed by RE at 830 K and after annealing to ~950 K shows the coexistence of the same 3D phases, namely, $NiSi_2$ and NiSi islands, as those formed by SPE at 1150 K, i.e., above the Ni solvus line. Our previous SPE study has already revised the accepted formation schemes for the Ni silicide phases and supported the earlier assumptions for existence of a metastable intermediate NiSi phase, structurally similar to the final $NiSi_2$ phase. The present results show that this also occurs when the interface is formed by RE at temperatures below the Ni solvus line. Another important resemblance is that independently of the formation temperature the $NiSi_2$ islands show the same directional orientation supporting our idea for anisotropy of the $NiSi_2$ nucleation barrier.[5] In our previous report we suggested that the enhanced Si mobility along structural irregularities (e.g., steps) with edges aligned with the $\langle 110\rangle$ direction facilitate the conversion of NiSi to $NiSi_2$, whereas onto the terraces the NiSi islands dominate. The important role of the Si mass transport for nucleation of the $NiSi_2$ islands is best manifested by the different thickness of the segregated Si layer on top of the $NiSi_2$ and the NiSi islands.

Despite the general resemblance there are differences between the interfaces formed below and above the Ni solvus line that are distinctive at a microscopic scale. These differences are revealed by examination and comparison of the spatial variations in the composition of the out-of-the-islands areas. The interface formed by SPE at 1150 K, (1×1)-RC phase with 3D islands, contained a distinct Ni-depleted zone, a ring ~3 μm wide, around all islands.[5] Parikh, Lee, and Bennett have pointed out that the (1×1)-RC has a lower surface energy but a higher kinetic barrier to formation than $\sqrt{19}$ and dominates at high formation temperatures.[2] Here for the initial $\sqrt{19}$ interface formed at 830 K broad lower Ni concentration regions are clearly formed in the areas with a higher density of NiSi islands, whereas the surface phase Ni content is the highest and without distinct depletion zones in the areas with high $NiSi_2$ island density [Fig. 1(a)]. This result indicates that at a lower formation temperature the Ni transport, in addition to that of Si, becomes important. For the $\sqrt{19}$ interface, formed at a constant temperature and Ni flux, the Ni mobility appears to be slower in the areas where the Si mobility is faster. It has to be attributed to the different mass transport mechanisms of Ni and Si: in contrast to Si atoms the transport of Ni atoms occurs predominantly via subsurface interstitial diffusion paths.[14] A reasonable interpretation is that at the initial RE formation temperatures of 830 K, the subsurface interstitial diffusion of Ni in the $\sqrt{19}$ phase has a higher activation barrier at the areas with surface irregularities. Another important result is that, in contrast to the case of a SPE formed interface at 1150 K, converting the areas away from the island from $\sqrt{19}$ into (1×1)-RC structure by annealing to 1000 K results in a rather homogeneous 2D phase without distinct depletion rings around the islands. The fact that a local depletion of Ni around the islands was not observed upon annealing to 1000 K, but occurred in the cases when the interface was formed by annealing to temperatures above the Ni solvus line, suggesting that dragging away Ni from the formed rather stable (1×1)-RC surface structure is a very slow process at 1000 K. This indicates that the mechanism of the Ni mass transport should be different for the (1×1)-RC and $\sqrt{19}$ phases. Reasonable interpretation is that the diffusing species in the case of the more stable (1×1)-RC structures are Ni containing ring clusters,[15] which are less mobile than the Ni atoms in the $\sqrt{19}$ phase.

V. CONCLUSIONS

A detailed and quantitative microcharacterization of the phases coexisting in the initial stages of Ni silicide growth reveals that the formation and coexistence of NiSi and $NiSi_2$ islands is a common phenomenon and readily occurs in the temperature range 800–1170 K. It has been found that at temperatures up to 830 K there is a correlation between the Ni coverage within the $\sqrt{19}$ ordered structure and the local density of the NiSi islands, attributed to lateral variations in the Ni and Si mobility. For the (1×1)-RC structure a local depletion of Ni around the islands is negligible at temperatures up to ~1000 K suggesting different type of diffusing species.

ACKNOWLEDGMENTS

We would like to thank Diego Lonza for the excellent technical assistance. The work was supported by Sincrotrone Trieste SCpA and in part by EC grants under Contract Nos. ERBCHGECT920013 and ERBFMBICT972391. R.J.P. was supported by The Laboratory for Physical Sciences, a University of Maryland International Exchange Grant, and in part by an NSF-MRSEC.

[1] H. von Kanel, Mater. Sci. Rep. **8**, 193 (1992).
[2] S. A. Parikh, M. Y. Lee, and P. A. Bennett, Surf. Sci. **356**, 53 (1996); , J. Vac. Sci. Technol. **13**, 1589 (1995).
[3] P. A. Bennett, M. Y. Lee, S. A. Parikh, K. Wurm, and R. J. Phaneuf, J. Vac. Sci. Technol. A **13**, 1728 (1995).
[4] A. E. Dolbak, B. Z. Olshanetsky, S. I. Stenin, S. A. Teys, and T. A. Gavrilova, Surf. Sci. **247**, 32 (1991).
[5] L. Gregoratti, S. Günther, J. Kovac, L. Casalis, M. Marsi, and M. Kiskinova, Phys. Rev. B **57**, R6799 (1998).
[6] M. Marsi, L. Casalis, L. Gregoratti, S. Günther, A. Kolmakov, J. Kovac, D. Lonza, and M. Kiskinova, J. Electron Spectrosc. Relat. Phenom. **84**, 73 (1997).
[7] M. P. Seah and W. A. Dench, Surf. Interface Anal. **1**, 2 (1970).
[8] S. Gunther, A. Kolmakov, J. Kovac, and M. Kiskinova, Ultramicroscopy (to be published).
[9] T. Barr, in *Modern ESCA: The Principles and Practice of X-ray Photoelectron Spectroscopy* (CRC, Boca Raton, FL, 1994), p. 93.
[10] A. R. Miedema, Z. Metallkd. **69**, 455 (1978); **69**, 287 (1978).
[11] V. Hinkel, L. Sorba, H. Haak, and K. Horn, Appl. Phys. Lett. **50**, 1257 (1987).
[12] F. J. Himpsel, B. S. Meyerson, F. R. McFeely, J. F. Morar, A. Taleb-Ibrahimi, and J. A. Yarmoff, in Proceedings of the International School of Physics ''Enrico Fermi,'' Course CVIII, edited by M. Campagha and R. Rosei (Elsevier, Amsterdam, 1990), p. 203.
[13] A. Franciosi *et al.*, Phys. Rev. B **26**, 546 (1982).
[14] M. Y. Lee and P. A. Bennett, Phys. Rev. Lett. **75**, 4460 (1998).
[15] R. J. Phaneuf, Y. Hong, S. Horch, and P. A. Bennett, Phys. Rev. Lett. **78**, 4605 (1997).